NACA RM No. L9B28

NACA

RESEARCH MEMORANDUM

INVESTIGATIONS OF AN ANNULAR DIFFUSER-FAN COMBINATION HANDLING ROTATING FLOW

By

Ira R. Schwartz

Langley Aeronautical Laboratory
Langley Air Force Base, Va.

NATIONAL ADVISORY COMMITTEE
FOR AERONAUTICS

WASHINGTON

April 25, 1949

NACA RM No. L9B28

NATIONAL ADVISORY COMMITTEE FOR AERONAUTICS

RESEARCH MEMORANDUM

INVESTIGATIONS OF AN ANNULAR DIFFUSER-FAN COMBINATION HANDLING ROTATING FLOW

By Ira R. Schwartz

SUMMARY

Two annular diffusers of different conical angles of expansion but constant outer diameters have been investigated with rotating flow behind a fan. The performance characteristics have been determined and the rotational-kinetic-energy effects on the over-all energy transformation were observed over a range of inlet Mach numbers from 0.1 to 0.55 and at angles of flow up to 28°. A wide range of flow distributions was encountered as a result of changes in operating conditions. The over-all performance of the 8° diffuser is shown to be substantially better than that of a 16° diffuser under comparable conditions for the range of Mach numbers and angles of rotation tested. Regions of maximum efficiency were found at angles of inflow approximately equivalent to the conical angle of expansion of the diffusers and again under conditions approaching axial flow. Sharp reductions in efficiency were recorded in both diffusers at the maximum values of stream rotation. The radial pressure gradient caused by the rotation of air assisted divergence of the flow; however, at the large angles of rotation, an adverse condition resulted from the inflow of low-energy air which in turn caused separation of flow on the inner wall. The rotational-kinetic-energy loss was negligible at the low angles but became appreciable at the maximum angle for low Mach numbers. This loss was greater for the 8° diffuser, but the over-all diffuser efficiencies remained higher than those of the 16° diffuser for corresponding test conditions.

INTRODUCTION

Diffusers for aircraft may be required to operate behind fans and turbosuperchargers which discharge the flow with considerable rotation from the annulus. It appears probable that the aerodynamic performance of such systems will be strongly influenced by the presence of this rotational component of flow. Of the great mass of diffuser performance data available, relatively little is directly applicable to aircraft problems dealing with rotating flows.

Vüllers (reference 1) in 1933, exploring the performance of rectangular diffusers for heating and ventilating application reported variations in efficiency with degree of rotation, and indicated the existence of a value of rotation for which the efficiency was a maximum. Peters (reference 2) studied the performance of conical diffusers under conditions approaching solid-body rotation. In these experiments both the inlet velocity profile and the degree of rotation were varied separately with a maximum inlet Mach number of about 0.12. For the conical diffuser with solid-body rotation Peters concluded that, "A comparison with the efficiency in pure axial flow reveals a marked increase as the spiral becomes more intense." Patterson (reference 3) discussed the work of previous experimenters and concluded that the vortex rotation produced by fans tends to improve the efficiency of ordinary diffusers when the rotation is small.

The independent variables in the flow characteristics at the diffuser inlet such as the velocity profiles and the turbulence factor have a combined influence on the energy transformation in the diffuser. Complete analysis of the individual factors influencing the performance of a diffuser in this type of flow is not feasible nor is it apparent that the mutual interference effects would not be of greater magnitude than the individual effects. The current research, therefore, was undertaken to determine the combined effect of all the variables over a representative range of operating conditions. In order to accomplish this, performance measurements were made of two annular diffusers, operating in flows generated by a representative axial fan.

The investigation was conducted in the Langley induction aerodynamics laboratory of the National Advisory Committee for Aeronautics using two annular, straight-wall diffusers with constant outside diameters and with conical inner bodies. One diffuser had an 8° and the other a 16° equivalent conical angle of expansion; the area ratio of both was 1.9. Stream Mach numbers ranging from 0.1 to 0.55 and a range of inlet angles of rotation from 0° to 28° were included in the test conditions.

The Reynolds numbers for the range of tests included in the subject research were 0.35×10^6 to 1.79×10^6. The method of calculation is presented in the appendix.

SYMBOLS

c	velocity of sound, feet per second
F_c	compressibility factor
H	total pressure, pounds per square foot or centimeters of alcohol, as indicated

M	Mach number (V/c)
m	mass flow, slugs per second
p	static pressure, pounds per square foot or centimeters of alcohol, as indicated
q	dynamic pressure, pounds per square foot
R_e	Reynolds number
r	radius
V	velocity of air in diffuser, feet per second
η	diffuser efficiency $\left(1 - \frac{\Delta\bar{H}}{\Delta\bar{q}}\right)$
θ	polar angle along circumference of duct, degrees
μ	coefficient of viscosity, slugs per foot-second
ρ	density of air, slugs per cubic foot
ψ	angle of rotation in air flow, degrees
ΔH	total pressure loss, pounds per square foot
Δp	change in static pressure, pounds per square foot
Δq	change in dynamic pressure, pounds per square foot
$\frac{\Delta\bar{H}}{\bar{q}_1}$	loss coefficient

Subscripts:

a	axial
r	resultant
i	inner conical body
o	outer duct wall
1	inlet station

2 exit station

ref reference station upstream of fan

Bar over symbol indicates a weighted average quantity.

APPARATUS

The experimental equipment used is shown in figures 1 and 2. The equipment consisted primarily of two annular straight-wall diffusers of constant outside diameter and area ratio, 1.9 to 1, figure 3. All internal surfaces were filled and polished.

The air entered the setup through a 48-inch-diameter screened bell inlet to distribute the air evenly to the annulus. The air passed through the annulus to the fan and then entered the test section. A 24-blade single-stage axial-flow fan, reference 4, was used to impart the rotation to the air flow. The blades were RAF 6 section, had maximum thickness of 12 percent of the chord and set at 63° from plane of rotation. The mass flow of air passing through the setup was controlled by an exhauster which was connected to the ducting at the exit of the diffuser.

Inlet and exit cross-sectional pressures and flow angles were measured by a remote-controlled survey rake shown in figures 4(a) and 4(b). The rake contained a total-pressure tube, a static tube and two yaw tubes. All readings were recorded after the rake was alined with the flow. The rake tubes were connected to a multiple-tube manometer board. Measurements were made at three inlet stations, 120° apart, and three exit stations 120° apart, figure 5. In addition to the rake measurements three outer wall statics were taken at the inlet and exit stations on the same plane with the rake.

In the diffuser section, wall static orifices were placed along the length on the outer duct wall and the conical inner body wall. The statics were placed in line with the rake positions, therefore giving three rows of static orifices (12 per row) 120° apart along the outer duct wall and three rows (13 stations per row) of inner-body wall statics 120° apart as indicated by figures 4(a) and 5. Stagnation air-stream temperatures were measured in front of and behind the fan by thermocouples connected to a sensitive potentiometer.

PROCEDURE

The test conditions were established by recording data at various fan speeds at a given flow Mach number. For comparison purposes the same fan speeds were used for each Mach number, the range of fan speeds

depended upon the limitations of the fan motor. For every fan speed at a given Mach number, the static and total pressures and the angle of rotation were measured across the annulus at the three inlet and the three exit measuring stations. The exit conditions were not measured at the same time the inlet conditions were recorded because rakes installed at the inlet would disturb the flow downstream. Measurements at the inlet and exit were taken with reference to the total pressure behind the screen in the bell. Intermediate wall statics at the inlet and exit measuring stations were recorded to check the accuracy of the static-pressure traversing tube. After the flow conditions at both inlet and exit stations were recorded, photographic records were made of the six lines of wall statics along the outer duct wall and the conical inner body wall. Air-flow temperatures were recorded for each test condition.

The following procedures have been used in the reduction of data presented herein: The angle of flow has been measured relative to a plane through the center line of the duct. All stream pressures have been measured with instrumentation alined with the flow. Mean values of angle and pressure were calculated from mass-weighted averages as indicated in the appendix. An average of the values at corresponding points for the three measuring stations was used to illustrate the pressure and flow angle distributions across the annulus of the duct. Two coefficients have been used in expressing diffuser performance, one a loss coefficient based upon the mean inlet dynamic pressure and the other diffuser energy efficiency based upon the measured difference in dynamic pressure at the inlet and exit.

$$\text{Loss coefficient} = \frac{\Delta\bar{H}}{\bar{q}_1}$$

$$\text{Diffuser energy efficiency} = 1 - \frac{\Delta\bar{H}}{\Delta\bar{q}} \quad \text{(See reference 5 and appendix.)}$$

The exit survey station was located somewhat downstream of the apex of the inner body cone in a region where the static pressure approached a maximum value. Wall static pressures presented are referenced to the mean inlet total pressure. The Reynolds number was calculated from the equation presented in the appendix which employs the hydraulic diameter of an annular section.

RESULTS AND DISCUSSION

The results of this investigation are given in tables I and II. Values of total and static pressure presented are referenced to the

total pressure upstream of the fan. Diffuser performance has been expressed as a loss coefficient $\frac{\Delta\bar{H}}{\bar{q}_1}$ and an energy efficiency $1 - \frac{\Delta\bar{H}}{\Delta\bar{q}}$ calculated for the resultant and axial components of velocity.

The performance of the 8° diffuser over the range of test conditions is shown in figure 6, which shows spot values of energy efficiency (η_r) on a field having mean flow angle as ordinate and inlet Mach number as abscissa. Graphs of the associated inlet velocity distribution, presented as the ratio of local velocity to mean velocity, are centered upon individual points for which efficiency is given. The top horizontal line of each square represents the inner body wall and the lower horizontal line represents the outer duct wall. The left-hand line of the square is a "0" reference line while the right-hand line denotes unity.

Although these data show certain irregularities in performance over the entire field, several definite trends can be established. In general the highest efficiencies ($\eta_r > 95$ percent) occurred at inlet rotational angles close to 8° and a secondary maximum with approximately axial inflow. Between these two regions, at $\bar{\psi} = 4°$, several values of η_r on the order of 80 percent were recorded. The only explanation for this result at 4° at the present is possibly a stall condition. Sharp reductions in efficiency were also noted at very high rotational angles. No clearly defined trend with Mach number at fixed angles of inflow could be established. It is not surprising that these irregularities should exist in view of the many variables in the flow that could influence boundary-layer phenomena and energy transformation.

The low efficiencies at the larger rotational inflow angles may be explained in the following manner: Although the radial pressure gradient caused by the rotation of the air assists the divergence of the flow, its effects are nullified by the centripetal flow of low-energy air which in turn induces flow separation on the inner wall. Typical curves of total and static pressure and flow angle are presented in figures 7, 8, and 9 for diffuser entrance Mach numbers of 0.1 and 0.4. With increasing mean angle of inlet flow the total-pressure distribution changed significantly; static-pressure and flow-angle distribution on the contrary were essentially constant throughout the range of this investigation for inlet conditions. The location of the total-pressure peaks can be correlated with the theory for this type of flow that the kinetic energy and rotational velocity are a maximum at the center of the duct and are small in comparison near the walls. The circulation is assumed to be constant at the diffuser inlet.

In many installations the flow distribution at the exit is of considerable importance. At a Mach number of 0.1 the total pressures across

the exit, figure 7, indicate increasing loss along the inner wall as the mean inlet angle increased, and a general shifting of the flow toward the outer wall. At a Mach number of 0.4, large losses in total pressure occurred along both duct walls but within the range of these tests no change in general shape of the curves occurred. The static pressure in the exit, figure 8, decreased smoothly from the outer to the inner wall, the magnitude of the difference in pressure increasing with angle of inlet flow. Although an extensive boundary-layer investigation was not conducted, tuft surveys and the pressure distributions indicate that these losses near the walls at the high angles are probably due to boundary-layer separation. Comparison of the curves of flow angle at the inlet and exit, figure 9, shows a marked increase in rotation as the air was slowed down. This effect indicates that the angular momentum is generally constant and any slight loss of momentum is due to viscous action as expected. Preliminary friction-coefficient calculations indicated that the viscous forces are small. The increase in mean angle of flow at the low velocity shown in figure 9 was accompanied by a change in distribution from relatively uniform rotation in the inlet to a nonuniform gradient with maximum angle of flow at the inner wall at the exit. It is noted that the maximum angle of flow and the lower values of total and static pressure occurred in the same region. At inflow angles of 17.8° and 28.3° the maximum angles near the inner body wall approached 90° which is an added indication that reversed flow due to boundary-layer separation appeared at the inner body wall.

The static-pressure distribution along both duct walls is shown for $M_1 = 0.1$ and 0.4 in figures 10(a) and 10(b), respectively. The decrease in static pressure at the base of the inner body cone indicates local acceleration of the flow. The decreasing static pressure over a large part of the cone at $\bar{\psi}_1 = 28^\circ$ is a result of increased rotation and loss of total pressure along the inner wall. Although the exact location of flow separation has not been determined for $\bar{\psi}_1 = 28^\circ$, experimental investigations showed that separation occurred well upstream in the vicinity where the static pressure begins to decrease. The static pressures in these plots serve another function in that they indicate the stage of energy transformation in the diffuser. In references 2 and 6 the authors have shown that the rise in pressure may not be complete at the final section of the diffuser and the necessity of adding discharge ducting for complete pressure conversion. The static pressures in figures 10(a) and 10(b) indicate that the energy transformation was complete or near complete and that no additional ducting was necessary. The few wall-static curves that indicate an incomplete pressure rise on the plots have been extrapolated by using the static pressure at the exit measuring station as an end point, and the slope of the final position of the extrapolated curves indicated complete pressure rise for all conditions. For rotating flow of this type the need for additional discharge length behind the diffuser exit is not as critical as for axial flow.

The efficiency of the 16° diffuser is shown in figure 11. Over a large part of the range of these tests the efficiency varied between 75 percent and 88 percent, with maximum values occurring at mean inlet angles of 2° and 15°. Values of efficiency less than 75 percent were obtained only at the very high values of inlet angle or Mach number. Comparison of these data with similar results from the 8° diffuser shows a range of differences in efficiency up to 20 percent, higher efficiency having been obtained with the 8° diffuser. These differences in efficiency may, in part, be caused by differences in inlet flow distribution at otherwise comparable conditions. As in the case of the 8° diffuser the highest efficiencies for the 16° diffuser were obtained for an inlet angle of flow approximately equivalent to its angle of diffusion. Because the 16° diffuser requires a large angle of rotation to reach its optimum efficiency, its over-all performance is not as efficient as a diffuser that can operate at a lower angle of rotation, a range where the rotation is beneficial to the diverging flow.

Typical curves of total pressure, static pressure, and angle across the inlet and exit of the 16° diffuser are presented in figures 12, 13, and 14. Inspection of these curves shows the same trends as were observed in the results of the 8° diffuser tests. In making these comparisons it should be kept in mind that the inlet and exit survey stations were the same in both tests, 48 inches from the inlet station. This system established the exit measuring station at 5 inches from the smallest diameter of the cone for the 8° diffuser and 24 inches for the 16° diffuser. The static pressures along both the inner and outer duct wall are presented in figures 15(a) and 15(b) for Mach numbers of 0.1 and 0.4. These curves bear a marked similarity to the curves for the 8° diffuser but have higher slopes. The negative slope of the pressure gradient along the cone in the 8° diffuser is also observed in the 16° diffuser but occurs first at a somewhat lower value of inlet angle.

The efficiencies are also presented in tables I and II as functions of the axial component of velocity or the change of kinetic energy in the axial direction. These efficiencies do not charge the diffuser with the loss of residual rotational energy.

A comparison of η_r and η_a shows that the rotational energy losses are negligible for both diffusers for angles of rotation up to 20°. For angles greater than 20° the rotational losses become appreciable at the low Mach numbers, M = 0.1 and 0.15. With an increase of Mach number, however, the losses appear to decrease for a constant angle of rotation. For the range of flow angles and Mach numbers tested the 8° diffuser has a higher over-all performance considering either η_r or η_a.

CONCLUDING REMARKS

The present investigation has led to several definite conclusions concerning the performance characteristics of a conical diffuser of this type handling rotating flow behind a fan and the influencing effects of rotational energy on the over-all energy transformation process. The over-all performance of the 8° diffuser was substantially higher than that of the 16° diffuser under similar inflow conditions and for Mach numbers through 0.55 and angles of rotation from 0° to 28°. Regions of high recovery were found with essentially axial flow and again at an angle approximately equivalent to the angle of expansion of the diffusers. The rotational energy losses are negligible at the small angles but become more appreciable for angles greater than 20° at low Mach numbers. The rotational energy losses are greater for smaller angular diffusers operating at low Mach numbers and high angles of rotation similar to those included in this investigation. Because of the large concentration of rotational kinetic energy in the center of the duct an adverse pressure gradient is established in flows near the inner wall, resulting in boundary-layer separation. In addition, it appears that the beneficial characteristics of a radial pressure gradient for diverging flow at the larger angles are nullified by the increased rotational kinetic energy that is not transformed to pressure.

Langley Aeronautical Laboratory
National Advisory Committee for Aeronautics
Langley Air Force Base, Va.

APPENDIX

COMPUTATION PROCEDURE FOR WEIGHTED AVERAGES, EFFICIENCIES, AND REYNOLDS NUMBER

The weighted total pressure is obtained from the relationship

$$\bar{H} = \frac{\int_0^{2\pi}\int_{r_i}^{r_o} H \, dm}{\int_0^{2\pi}\int_{r_i}^{r_o} dm} \tag{1}$$

$$= \frac{\int_0^{2\pi}\int_{r_i}^{r_o} H\sqrt{\frac{2\rho}{F_c}}\sqrt{H - p}\, r \, dr \, d\theta}{\int_0^{2\pi}\int_{r_i}^{r_o} \sqrt{H - p}\sqrt{\frac{2\rho}{F_c}}\, r \, dr \, d\theta} \tag{2}$$

$\bar{p}$, $\bar{q}$, and $\bar{\psi}$ are calculated in a similar manner.

The diffuser efficiency is determined by the amount of kinetic energy that is converted to potential energy. Efficiency is expressed as the rise of static pressure to the change of dynamic pressure.

$$\eta_r = \frac{\Delta\bar{p}}{\Delta\bar{q}} \tag{3}$$

From equation (3) an expression of efficiency is obtained which is used in this report

$$\eta_r = 1 - \frac{\bar{H}_1 - \bar{H}_2}{\bar{q}_1 - \bar{q}_2} \tag{4}$$

The efficiency η_a is obtained from the following equation:

$$\eta_a = 1 - \frac{\Delta\bar{H}}{\bar{q}_1 \cos^2\bar{\psi}_1 - q_2 \cos^2\bar{\psi}_2}$$

The Reynolds number is derived from the relationship

$$R_e = \frac{\rho V_1}{\mu} \times \text{Hydraulic diameter}$$

$$\text{Hydraulic diameter} = \frac{4 \times \text{Area of annulus}}{\text{Wetted perimeter}}$$

Therefore for an annular diffuser

$$R_e = \frac{\rho V_1}{\mu}(d_o - d_i)$$

REFERENCES

1. Vüllers, H.: Ausnutzung der kinetischen austrittsenergie der Luft bei Ventilatoren mittels Diffusoren. Z.V.D.I., vol. 77, no. 31, 1933. (Translation available in the Institute of Heating and Ventilating Journal, vol. 1, no. 8, Oct. 1933, p. 423.)

2. Peters, H.: Conversion of Energy in Cross-Sectional Divergences under Different Conditions of Inflow. NACA TM No. 737, 1934.

3. Patterson, G. N.: Modern Diffuser Design. Aircraft Engineering, vol. X, no. 115, Sept. 1938, pp. 267-273.

4. Bell, E. Barton: Test of a Single-Stage Axial-Flow Fan. NACA Rep. No. 729, 1942.

5. Becker, John V., and Baals, Donald D.: Analysis of Heat and Compressibility Effects in Internal Flow Systems and High-Speed Tests of a Ram-Jet System. NACA Rep. No. 773, 1943.

6. Gibson, A. H.: On the Flow of Water through Pipes and Passages Having Converging or Diverging Boundaries. Proc. Roy. Soc. (London), ser. A, vol. 83, no. 563, March 2, 1910, pp. 366-378.

TABLE I.- SUMMARY OF 8° DIFFUSER DATA

Mach number, M	Angle of rotation (deg)		Total pressure, H-Href (lb/sq ft)		Static pressure, p-Href (lb/sq ft)		Dynamic pressure, (lb/sq ft)		Change in pressure, (lb/sq ft)		Loss coefficient, $\frac{\Delta\bar{H}}{\bar{q}_1}$	Energy efficiency, η_r	Energy efficiency, η_a
	$\bar{\psi}_1$	$\bar{\psi}_2$	$\bar{H}_1$	$\bar{H}_2$	$\bar{p}_1$	$\bar{p}_2$	$\bar{q}_1$	$\bar{q}_2$	$\Delta\bar{H}$	$\Delta\bar{q}$			
0.10	1	5	-2.26	-2.92	-17.33	-7.93	15.07	5.01	0.66	10.06	0.04	0.93	0.93
.10	8	18	-.68	-.71	-15.48	-6.61	14.80	5.90	.03	8.90	.002	.99	.99
.11	18	38	5.38	4.40	-11.26	-3.12	16.64	7.52	.98	9.12	.06	.89	.91
.11	28	51	15.21	12.35	-4.17	-1.04	19.38	13.39	2.86	5.99	.15	.52	.71
.15	1	2	-6.14	-7.37	-39.09	-18.60	32.95	11.23	1.23	21.72	.04	.94	.94
.15	4	14	-2.11	-3.74	-36.58	-14.98	34.47	11.24	1.63	23.23	.05	.93	.93
.15	14	32	7.34	4.80	-27.52	-7.85	34.86	12.65	2.54	22.21	.07	.89	.89
.16	17	37	11.92	9.75	-24.44	-6.08	36.36	15.83	2.17	20.53	.06	.89	.91
.16	23	45	21.39	17.18	-17.43	-1.78	38.82	18.96	4.21	19.86	.11	.79	.82
.17	28	58	32.78	28.45	-9.85	4.15	42.63	24.30	4.33	18.33	.10	.76	.84
.20	1	5	-9.52	-12.74	-67.22	-31.50	57.70	18.76	3.22	38.94	.06	.92	.92
.20	7	18	-1.89	-3.00	-58.75	-24.83	56.86	21.83	1.11	35.03	.02	.97	.97
.21	10	24	6.37	3.39	-54.24	-17.32	60.61	20.71	2.98	39.90	.05	.93	.93
.21	14	32	13.12	10.14	-47.81	-14.30	60.93	24.44	2.98	36.49	.05	.92	.93
21	19	40	26.73	22.33	-38.47	-7.24	65.20	29.57	4.40	35.63	.07	.88	.89
.25	1	3	-15.47	-20.00	-106.10	-52.55	90.63	32.55	4.53	58.08	.05	.92	.92
.25	4	12	-5.88	-19.67	-99.55	-42.78	93.67	23.11	13.79	70.56	.15	.81	.81
.25	7	18	-1.98	-4.78	-91.97	-35.07	89.99	30.29	2.80	59.70	.03	.95	.95
.25	12	28	15.30	6.49	-78.46	-26.81	93.76	33.30	8.81	60.46	.09	.85	.86
.30	0	3	-21.24	-27.92	-149.62	-67.06	128.38	39.14	6.68	89.24	.05	.93	.93
.30	3	13	-8.00	-26.78	-138.80	-59.30	130.80	32.52	18.78	98.28	.14	.81	.81
.30	7	19	-2.41	-5.31	-127.62	-49.81	125.21	44.50	2.90	80.71	.02	.96	.97
.30	10	23	6.66	2.08	-122.38	-44.63	129.04	46.71	4.58	82.33	.04	.94	.95
.35	0	3	-30.26	-37.41	-202.51	-91.05	172.25	53.64	7.15	118.61	.04	.94	.94
.35	3	12	-8.59	-36.39	-187.21	-81.04	178.62	44.65	27.80	133.97	.16	.79	.79
.35	5	16	-7.90	-15.18	-180.55	-73.35	172.65	58.18	7.27	114.47	.04	.94	.94
.35	7	18	-4.14	-7.91	-174.16	-68.16	170.02	60.25	3.77	109.77	.02	.97	.97
.40	0	2	-41.00	-50.57	-264.62	-118.45	223.62	67.88	9.57	155.74	.04	.94	.94
.40	2	6	-30.73	-45.02	-253.64	-109.83	222.91	64.81	14.29	158.10	.06	.91	.91
.41	4	14	-5.17	-38.15	-238.05	-97.45	232.88	59.30	32.98	173.58	.14	.81	.81
.51	1	6	-51.83	-78.94	-393.71	-173.81	341.88	94.87	27.11	247.01	.08	.89	.89
.51	3	9	-36.75	-82.10	-375.73	-161.88	338.98	79.78	45.35	259.20	.13	.83	.83

TABLE II - SUMMARY OF 16° DIFFUSER DATA

Mach number, M	Angle of rotation (deg)		Total pressure, H-H_{ref} (lb/sq ft)		Static pressure, p-H_{ref} (lb/sq ft)		Dynamic pressure, (lb/sq ft)		Change in pressure, (lb/sq ft)		Loss coefficient, $\frac{\Delta\bar{H}}{\bar{q}_1}$	Energy efficiency, η_r	Energy efficiency, η_a
	$\bar{\psi}_1$	$\bar{\psi}_2$	$\bar{H}_1$	$\bar{H}_2$	$\bar{p}_1$	$\bar{p}_2$	$\bar{q}_1$	$\bar{q}_2$	$\Delta\bar{H}$	$\Delta\bar{q}$			
0.10	4	8	-2.09	-4.05	-17.44	-9.43	15.35	5.38	1.96	9.97	0.13	0.80	0.80
.10	10	20	0.54	-1.65	-15.01	-7.63	15.55	5.98	2.19	9.57	.14	.77	.78
.10	19	36	6.34	4.71	-10.56	-3.16	16.90	7.87	1.63	9.03	.10	.82	.84
.10	27	47	14.87	9.03	-4.61	1.19	19.48	7.84	5.84	11.64	.30	.50	.51
.15	3	6	-5.21	-8.35	-37.81	-18.86	32.60	10.51	3.14	22.09	.10	.86	.86
.15	7	14	-2.04	-7.42	-35.94	-17.70	33.90	10.28	5.38	23.62	.16	.77	.77
.15	16	32	7.67	4.70	-26.57	-9.90	34.24	14.60	2.97	19.64	.09	.85	.86
.15	19	36	14.40	10.41	-22.72	-6.79	37.12	17.20	3.99	19.92	.11	.80	.82
.15	23	42	22.43	19.09	-16.76	-0.78	39.19	19.87	3.34	19.32	.09	.83	.85
.15	28	48	33.55	29.42	-9.10	3.58	42.65	25.84	4.13	16.81	.10	.75	.81
.20	2	7	-9.42	-14.39	-67.97	-35.66	58.55	21.27	4.97	37.28	.08	.87	.87
.20	9	19	3.05	-5.23	-59.52	-26.61	62.57	21.38	8.28	41.19	.13	.80	.80
.20	12	24	6.50	0.22	-54.95	-22.45	61.45	22.67	6.28	38.78	.10	.84	.84
.20	15	32	13.63	9.51	-47.86	-15.59	61.49	25.10	4.12	36.39	.07	.89	.90
.20	19	38	29.73	22.51	-39.32	-7.87	69.05	30.38	7.22	38.67	.10	.81	.83
.25	2	6	-15.04	-22.29	-104.26	-51.88	89.22	29.59	7.25	59.63	.08	.88	.88
.25	6	13	-5.86	-20.54	-98.51	-46.52	92.65	25.98	14.68	66.67	.16	.78	.78
.25	10	19	5.90	-9.05	-89.00	-41.11	94.90	32.06	14.95	62.84	.16	.76	.76
.25	13	28	15.64	4.95	-77.23	-29.57	92.87	34.52	10.69	58.35	.12	.82	.83
.30	2	6	-22.17	-32.54	-152.00	-73.47	129.83	40.93	10.37	88.90	.08	.88	.88
.30	5	13	-9.71	-28.29	-140.61	-64.21	130.90	35.92	18.58	94.98	.14	.80	.81
.30	8	19	4.90	-10.70	-130.41	-55.90	135.31	45.20	15.60	90.11	.12	.83	.83
.30	11	23	10.02	-4.10	-124.40	-51.01	134.42	46.91	14.12	87.51	.11	.84	.84
.35	2	5	-14.72	-44.52	-199.05	-99.02	184.33	54.50	29.80	129.83	.16	.77	.77
.35	6	13	-9.44	-39.25	-187.77	-88.05	178.33	48.80	29.81	129.53	.17	.77	.77
.35	7	16	-1.98	-28.05	-179.03	-81.16	177.05	53.11	26.07	123.94	.15	.79	.79
.35	8	18	3.81	-21.40	-172.95	-77.85	176.76	56.45	25.21	120.31	.14	.79	.79
.40	2	4	-36.10	-61.41	-261.16	-126.47	225.06	65.06	25.31	160.00	.11	.84	.84
.40	3	8	-24.36	-51.23	-251.41	-118.09	227.05	66.86	26.87	160.19	.12	.83	.83
.40	5	14	-9.48	-50.66	-235.16	-112.09	225.68	61.43	41.18	164.25	.18	.75	.75
.51	1	3	-19.06	-123.48	-409.43	-202.38	390.37	78.90	104.42	311.47	.27	.66	.66
.51	3	8	-14.68	-95.76	-394.36	-198.16	379.68	102.40	81.08	277.28	.21	.71	.71

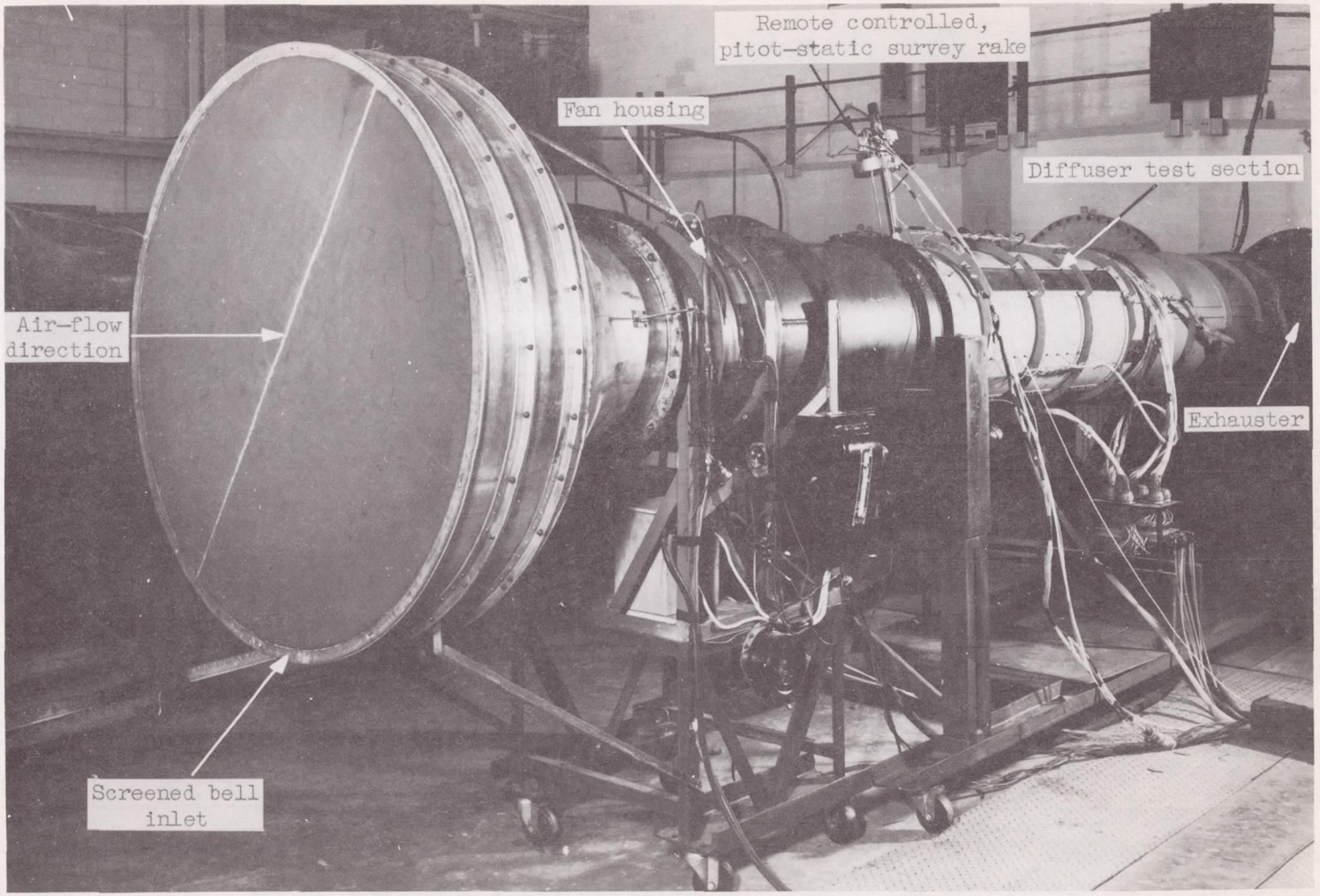

NACA
L-53624

Figure 1.- General view of test apparatus.

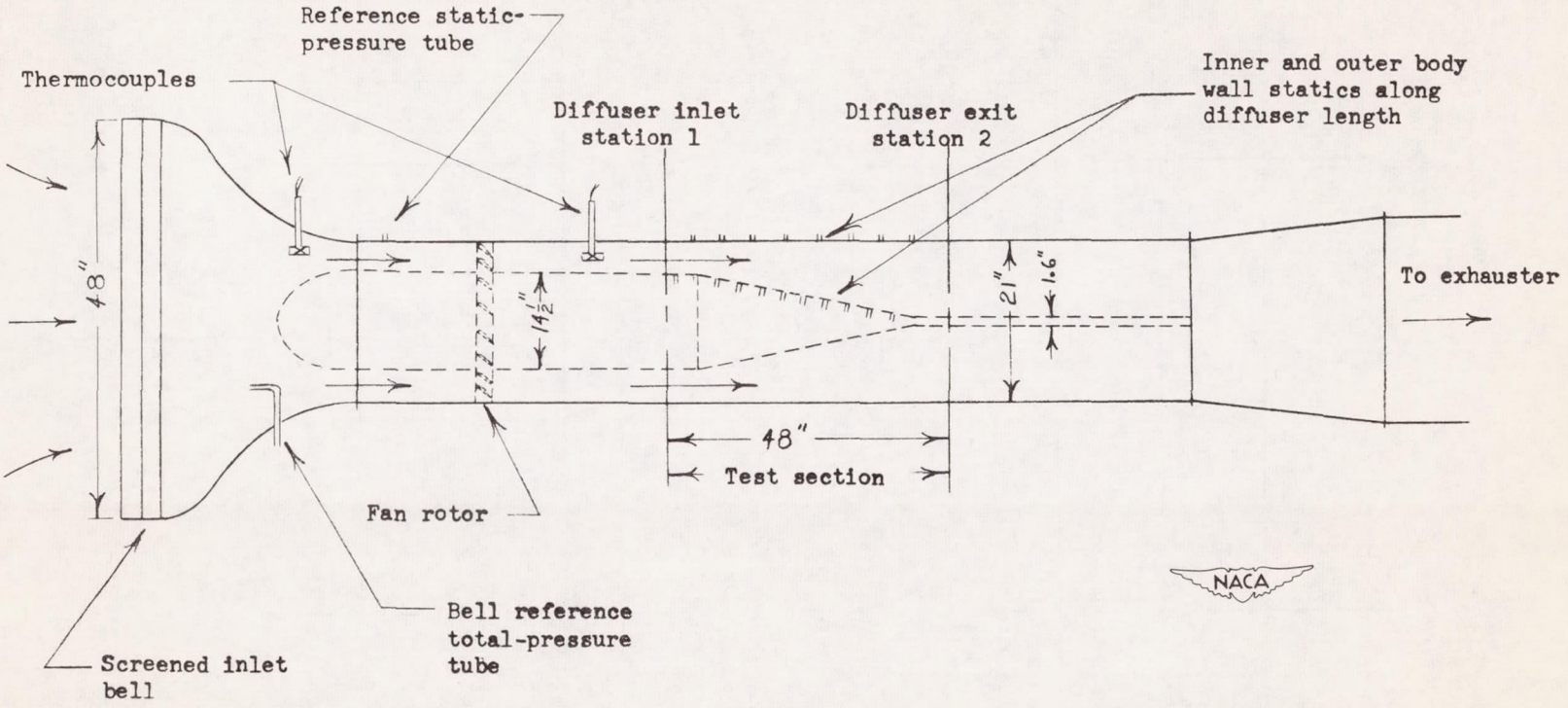

Figure 2.– Schematic diagram of experimental setup for tests of diffusers with rotational flow.

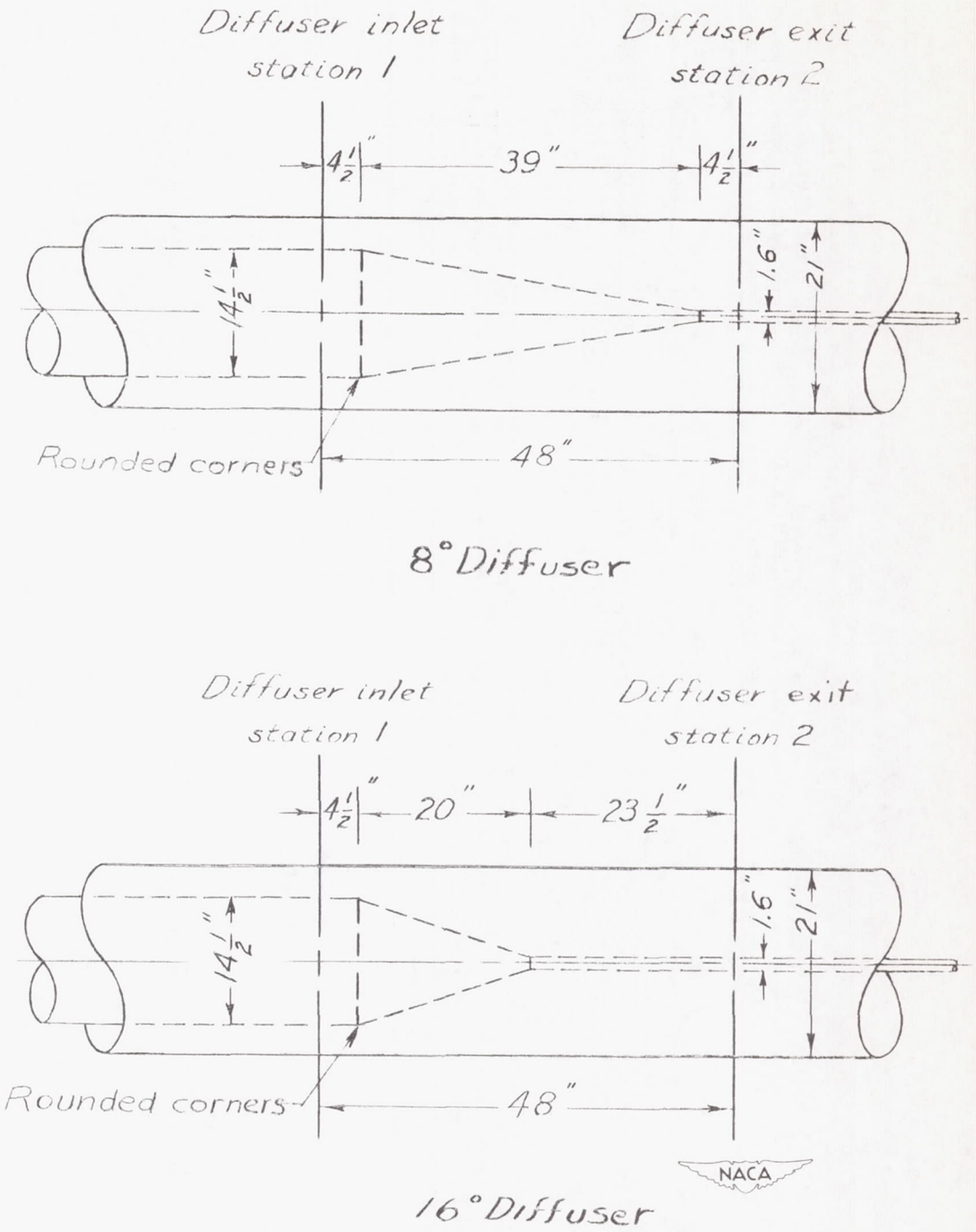

Figure 3.– Sketches and dimensions of the two annular diffusers tested.

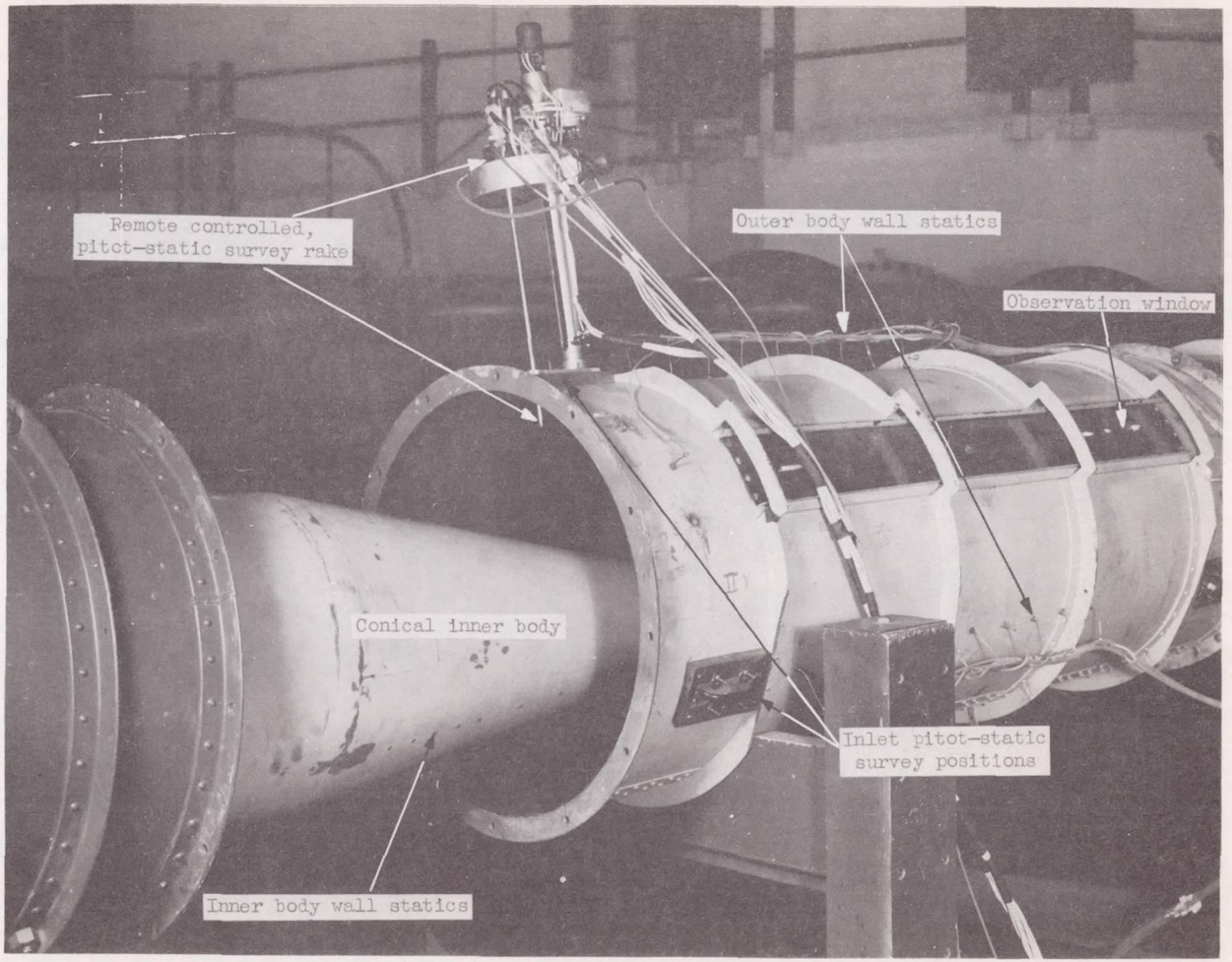

NACA
L-53609

(a) General view of installation.

Figure 4.- Remote-controlled survey rake.

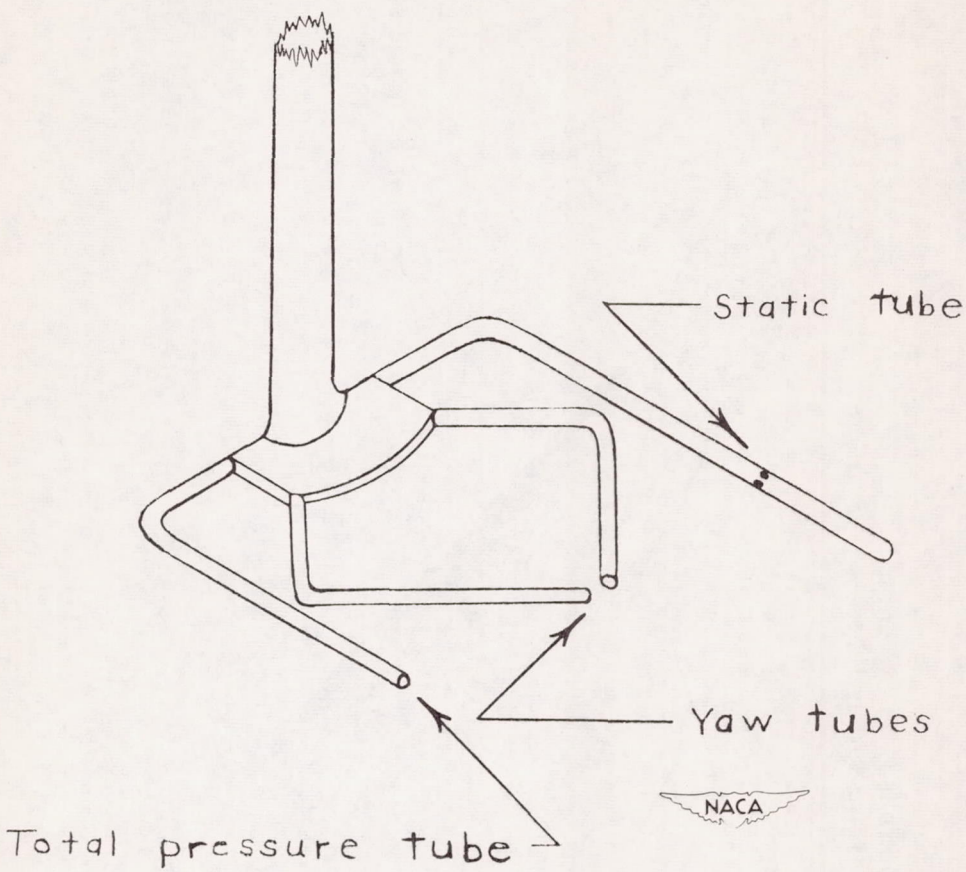

(b) Detail of survey rake.

Figure 4.– Concluded.

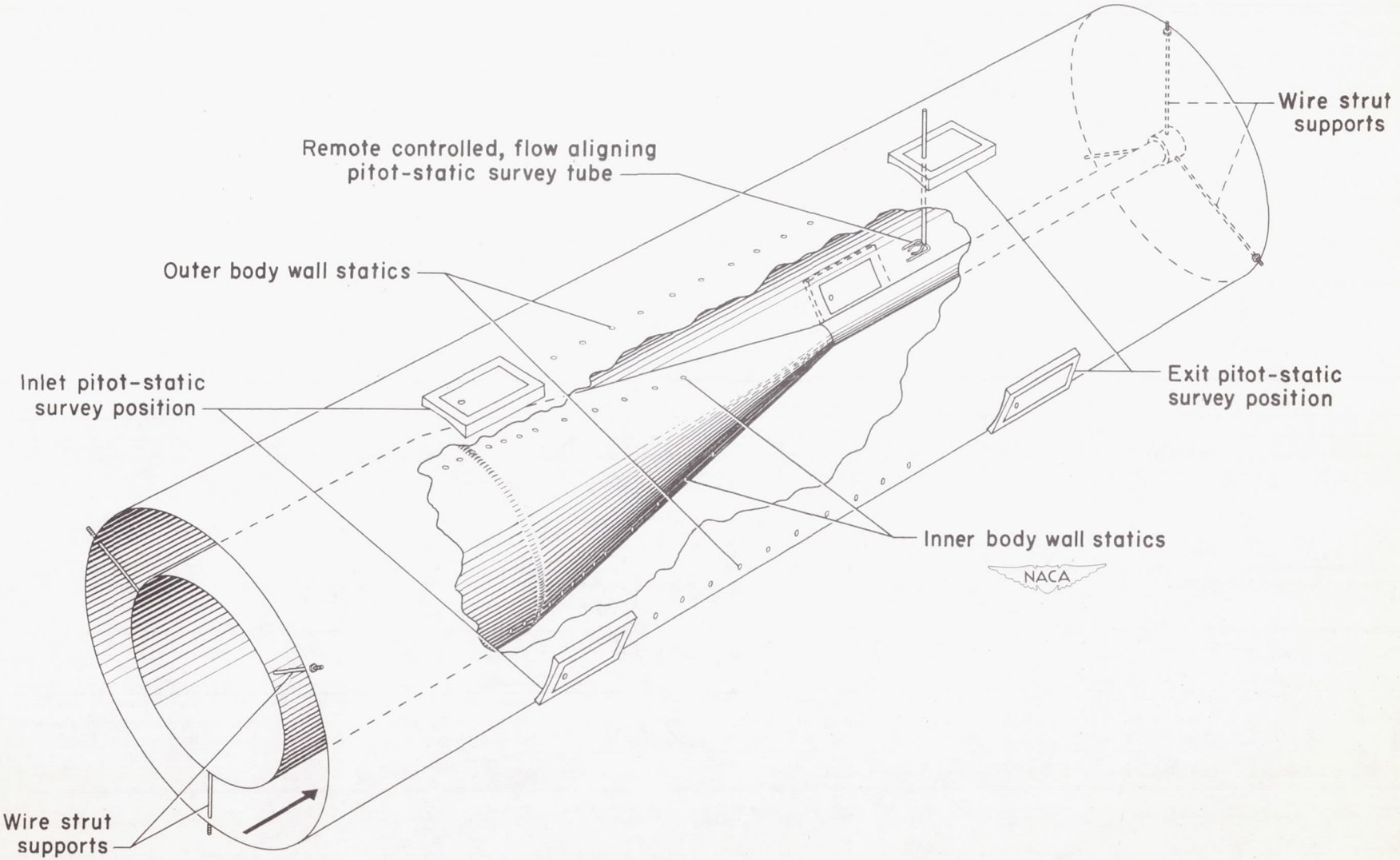

Figure 5.– General arrangement and instrumentation details of diffuser test section. The outer and inner body wall statics and inlet and exit survey positions are in circumferential alinement along diffuser length in 3 rows 120° apart.

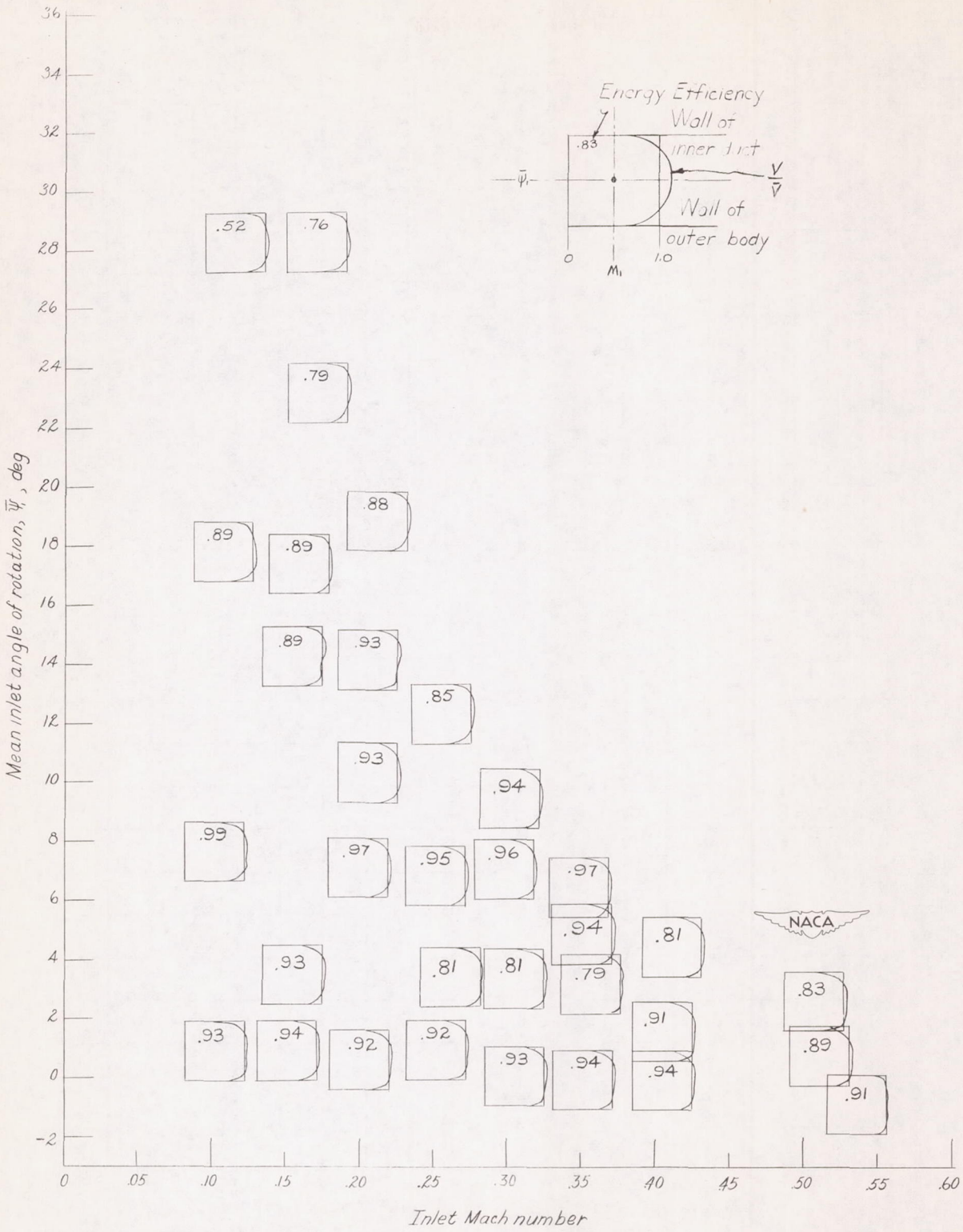

Figure 6.– Plots of diffuser energy efficiency and inlet velocity distributions of 8° diffuser for the range of inlet Mach numbers and angle of flows tested.

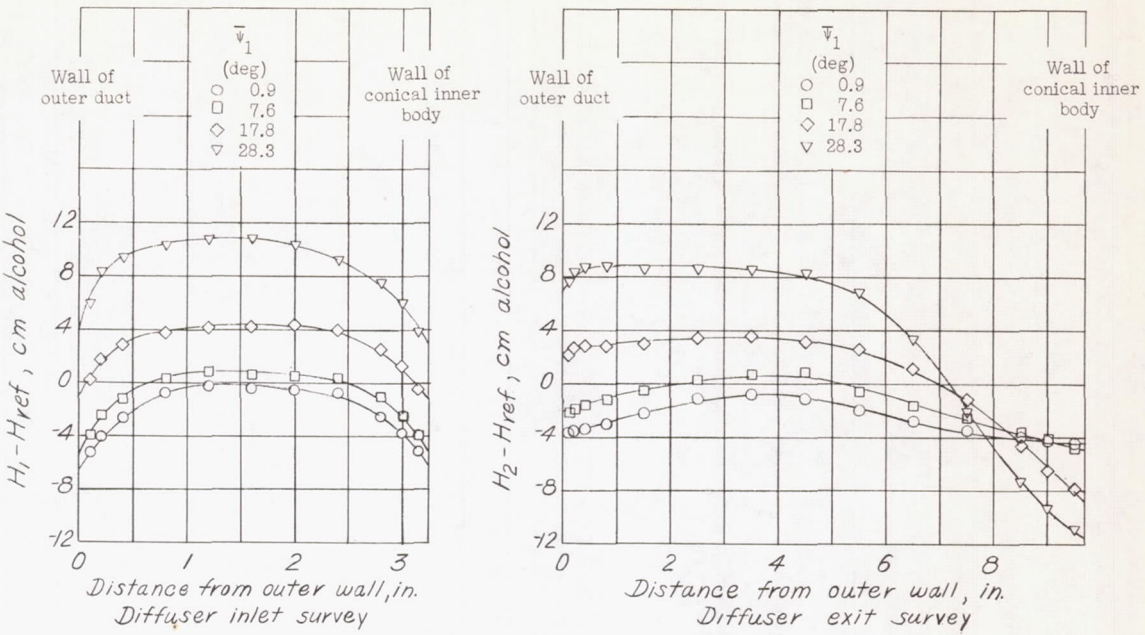

(a) Total-pressure distributions for a diffuser inlet Mach no. of 0.10.

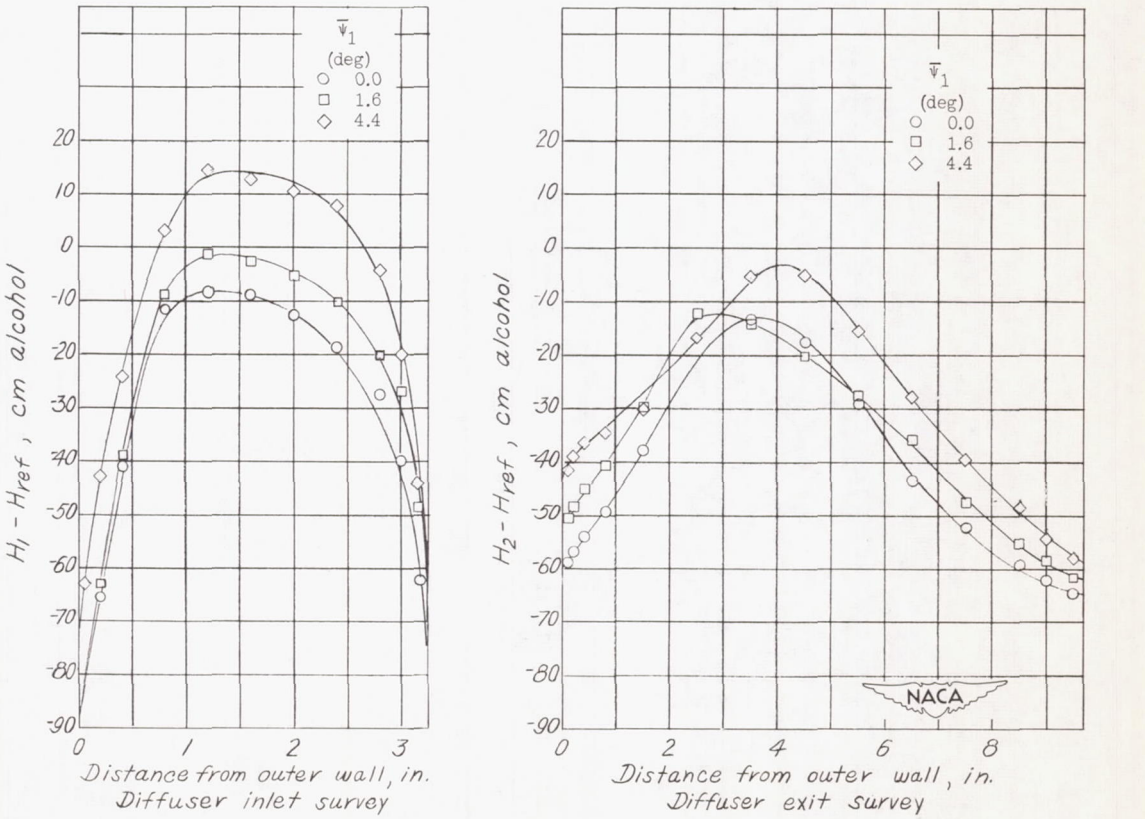

(b) Total-pressure distributions for a diffuser inlet Mach no. of 0.40.

Figure 7.– Plots of total–pressure–distribution surveys at the inlet and exit of the 8° diffuser.

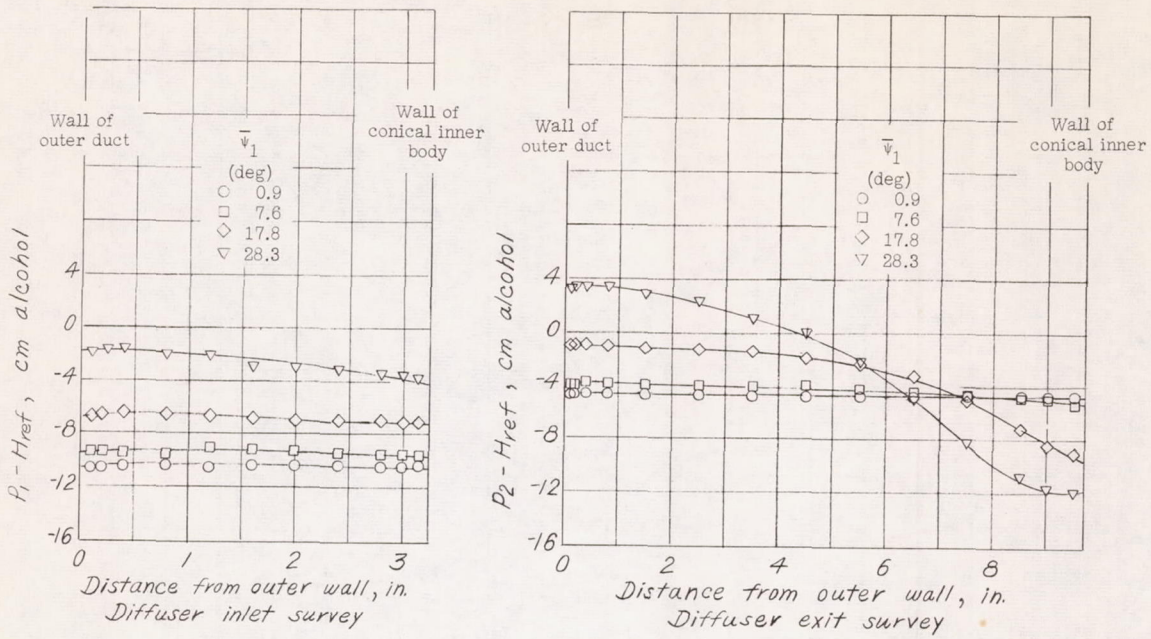

(a) Static-pressure distributions for a diffuser inlet Mach no. of 0.10.

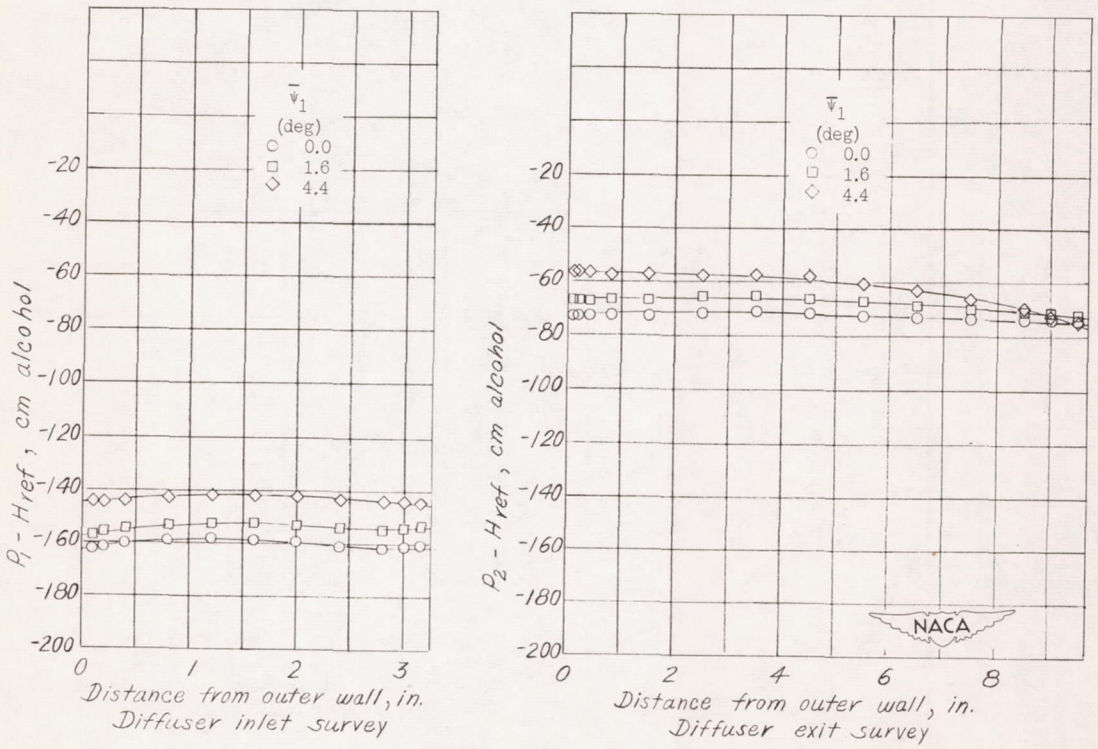

(b) Static-pressure distributions for a diffuser inlet Mach no. of 0.40.

Figure 8.- Plots of static-pressure-distribution surveys at the inlet and exit of the 8° diffuser.

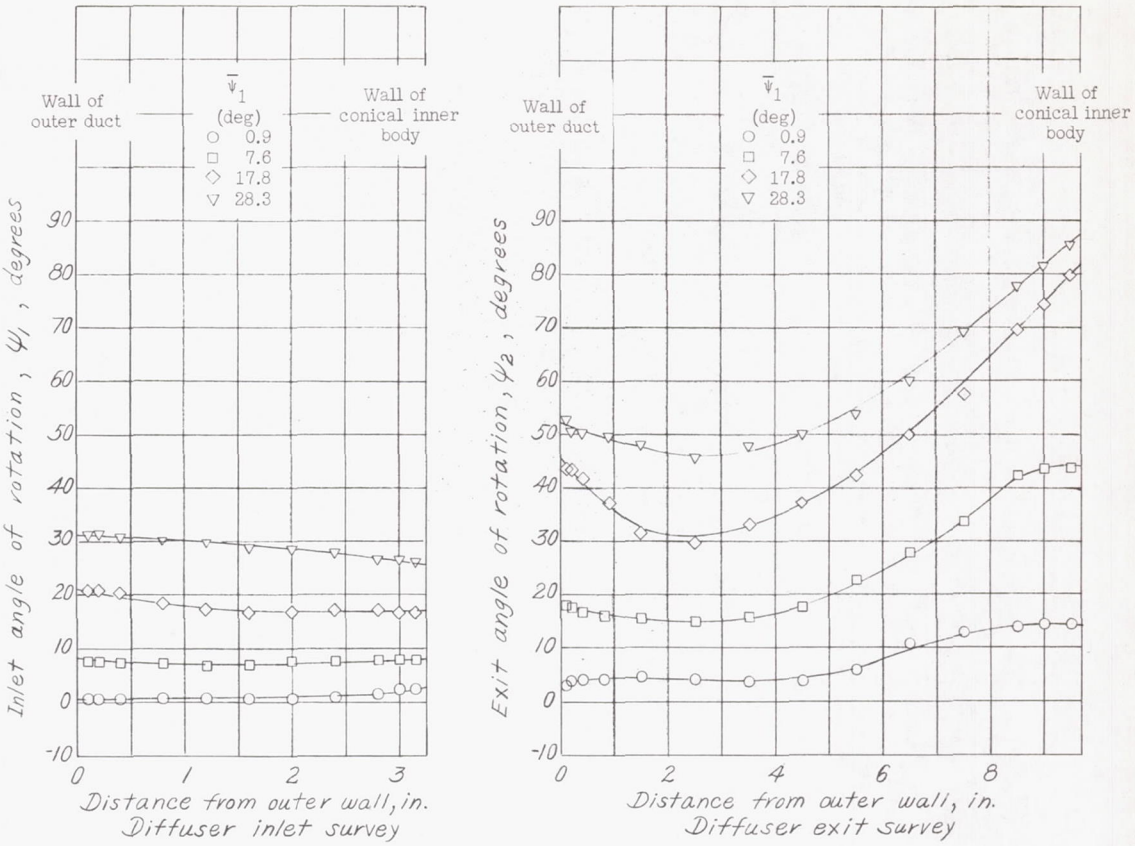

(a) Angle-of-rotation distributions for a diffuser inlet Mach no. of 0.10.

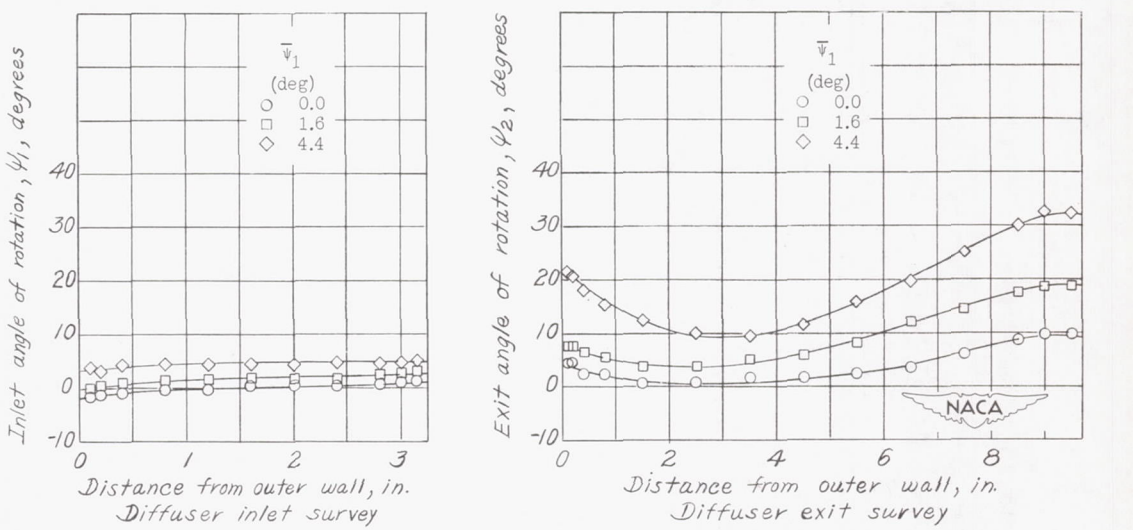

(b) Angle-of-rotation distributions for a diffuser inlet Mach no. of 0.40.

Figure 9.- Plots of angle of flow rotation at the inlet and exit of the 8° diffuser.

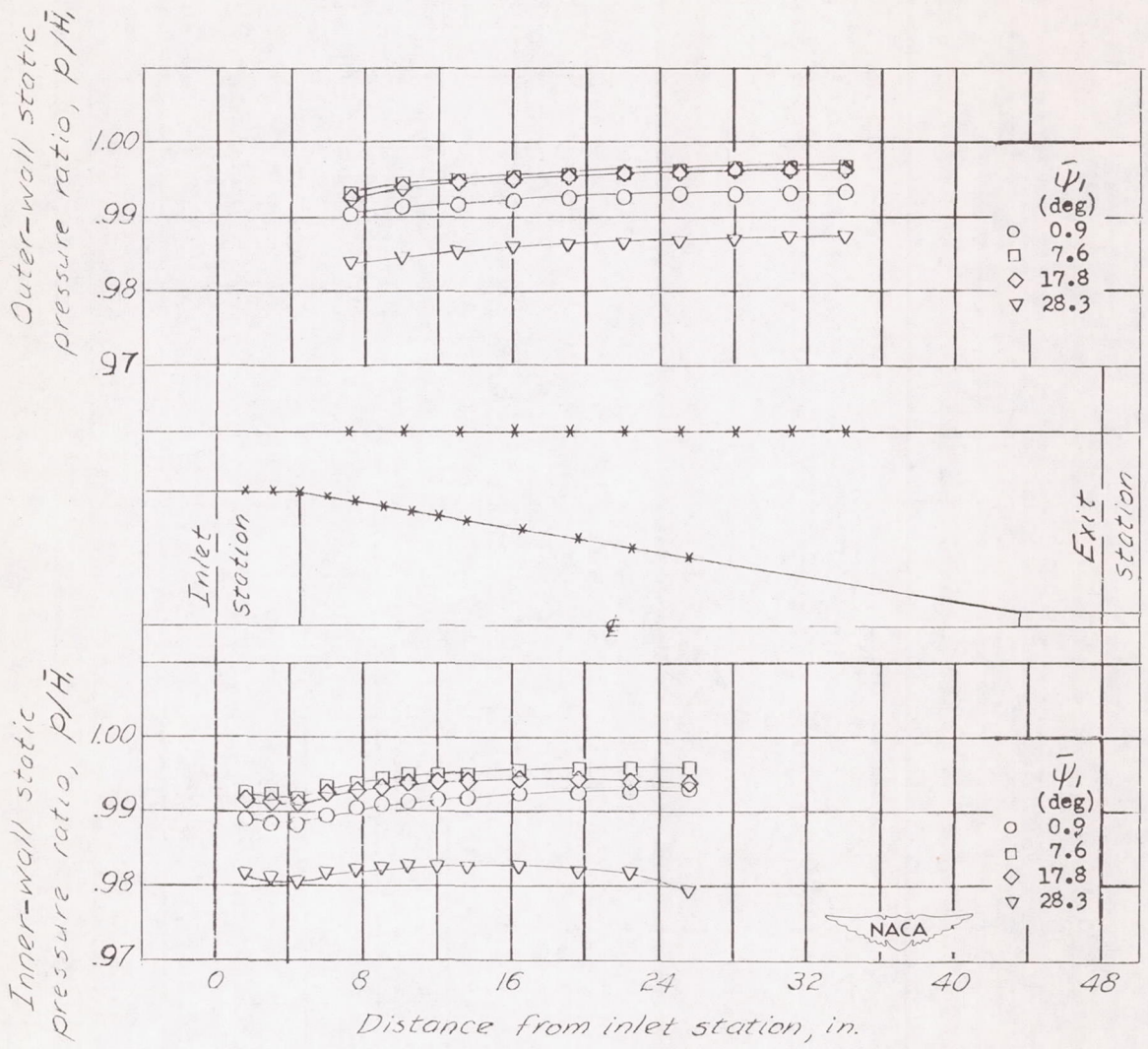

(a) $M_1 = 0.1$

Figure 10.– Plots of wall static pressures along inner conical body and outer duct for the 8° diffuser.

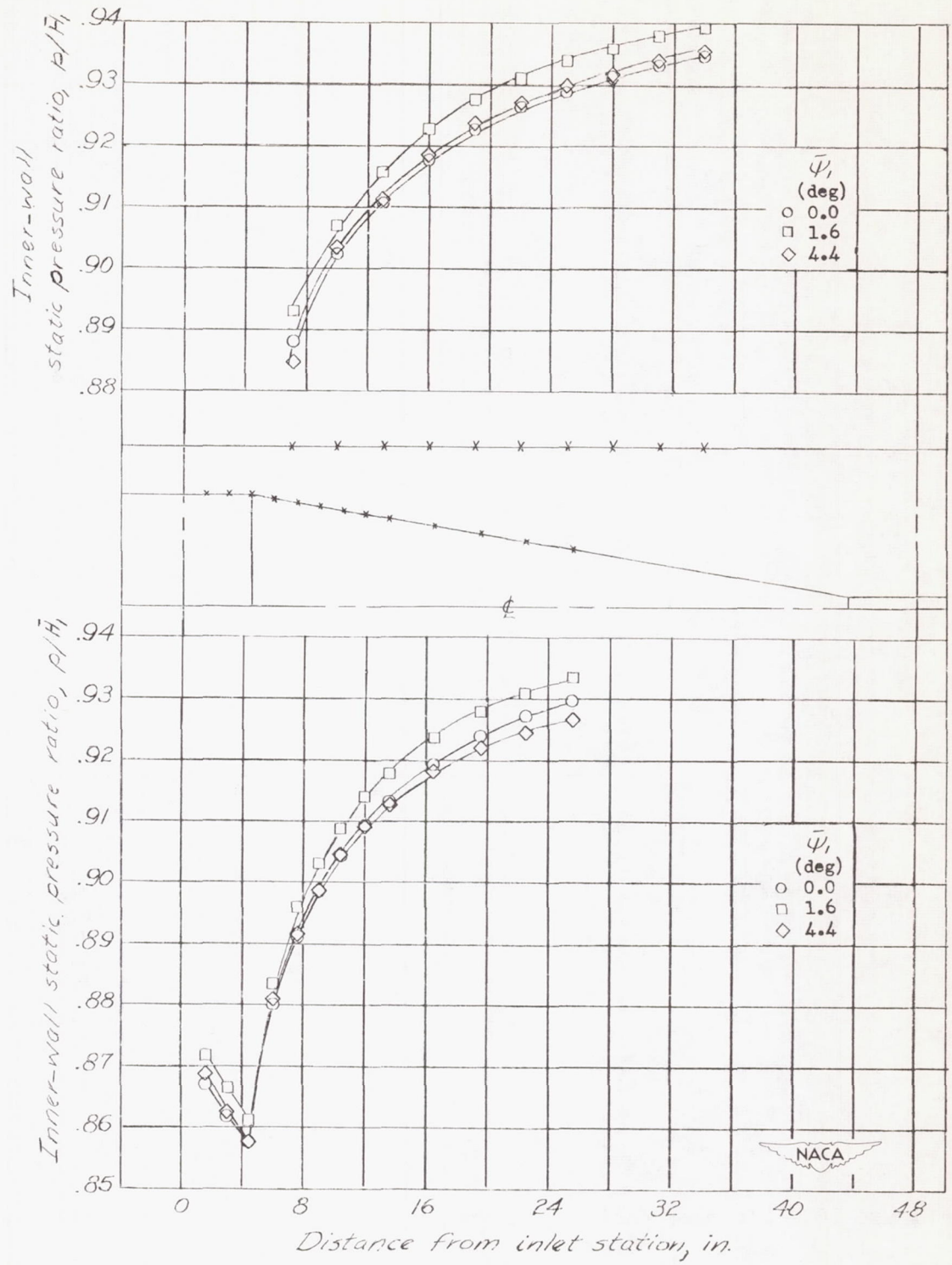

(b) $M_1 = 0.4$.

Figure 10.– Concluded.

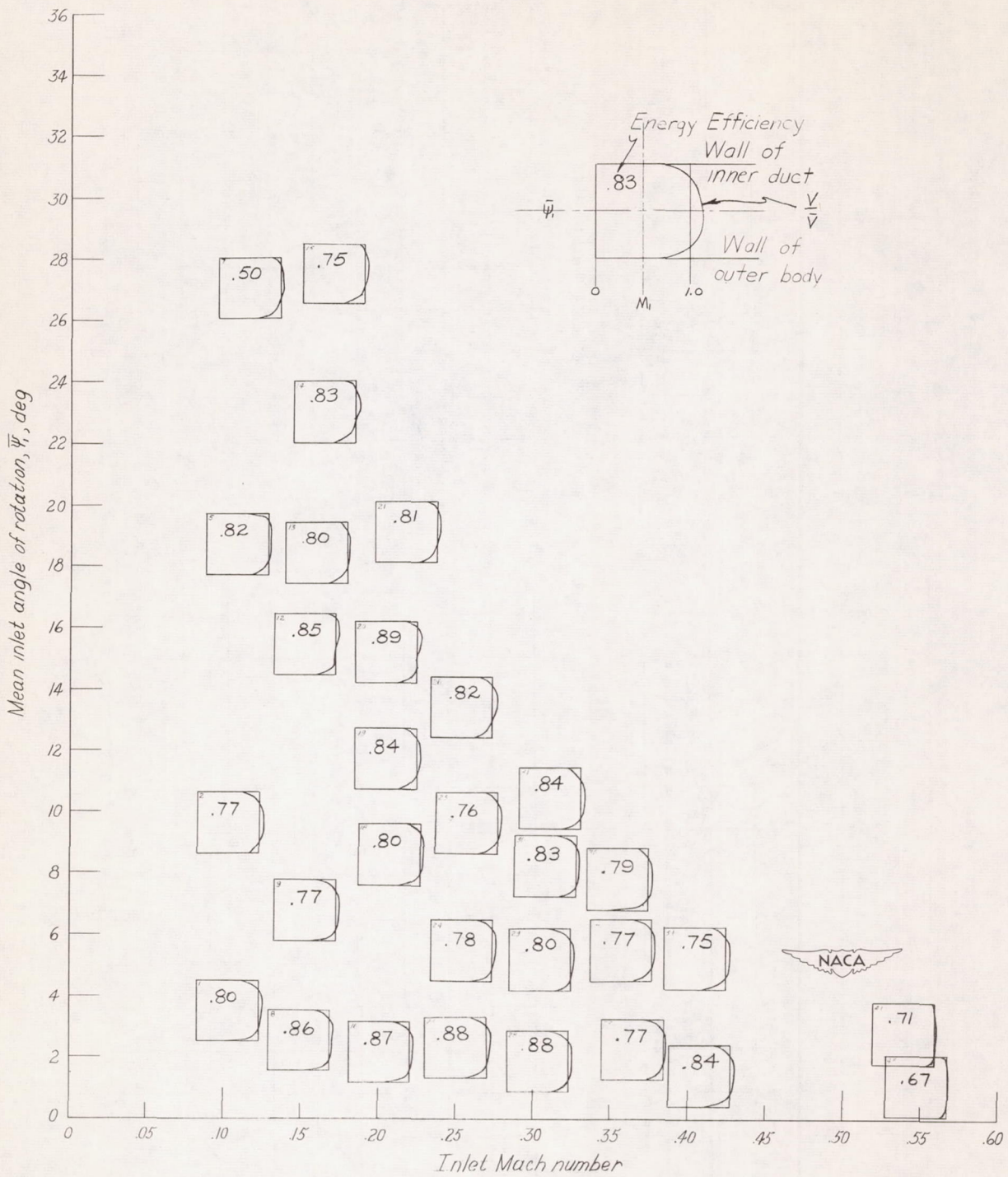

Figure 11.– Plots of diffuser energy efficiency and inlet velocity distributions of 16° diffuser for the range of inlet Mach numbers and angles of flow tested.

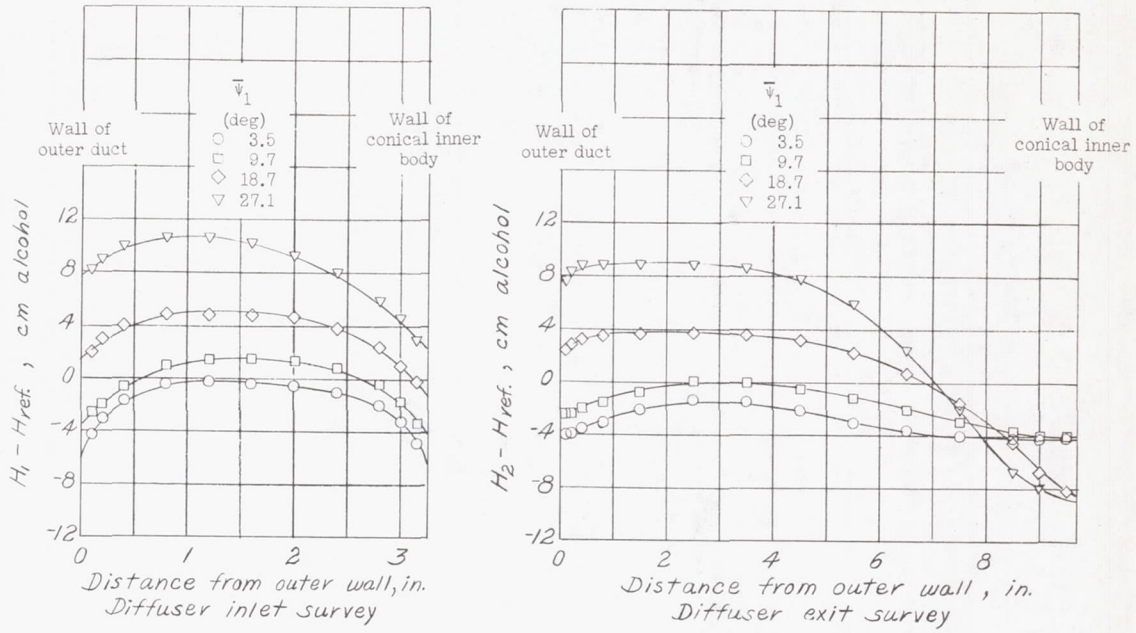

(a) Total-pressure distributions for a diffuser inlet Mach no. of 0.10.

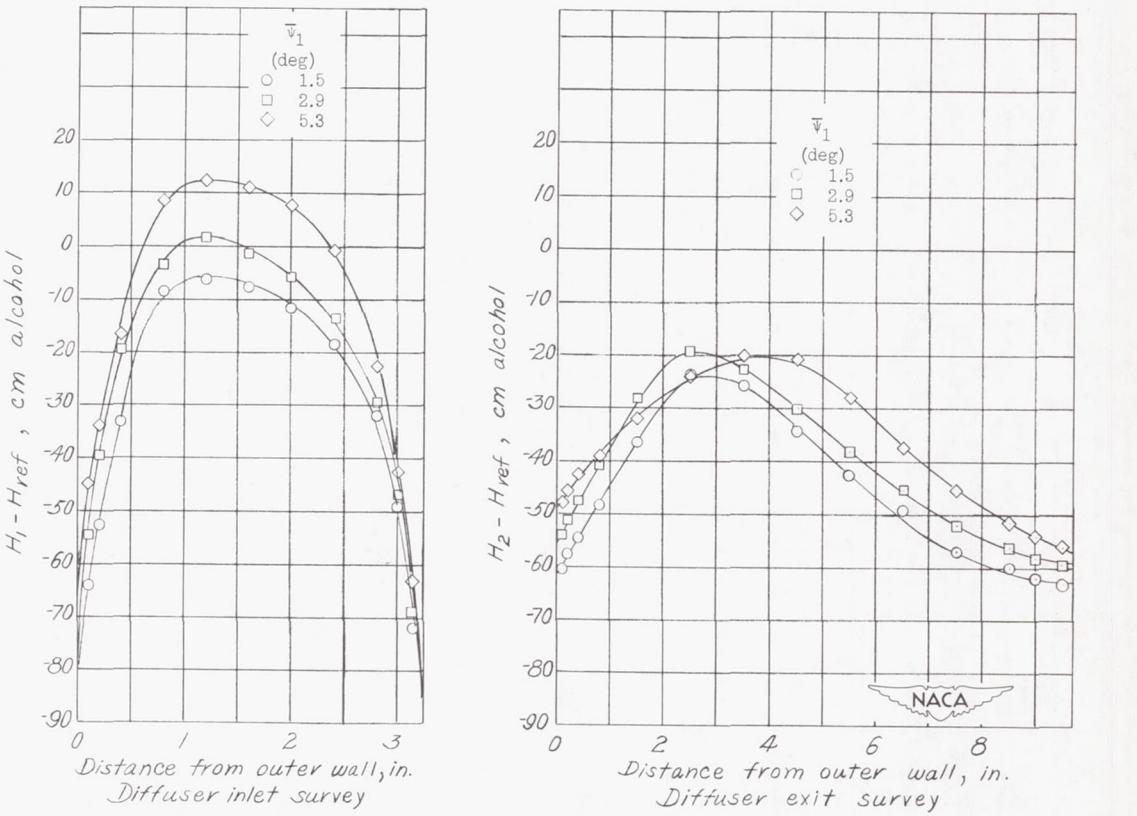

(b) Total-pressure distributions for a diffuser inlet Mach no. of 0.40.

Figure 12.– Plots of total–pressure–distribution surveys at the inlet and exit of the 16° diffuser.

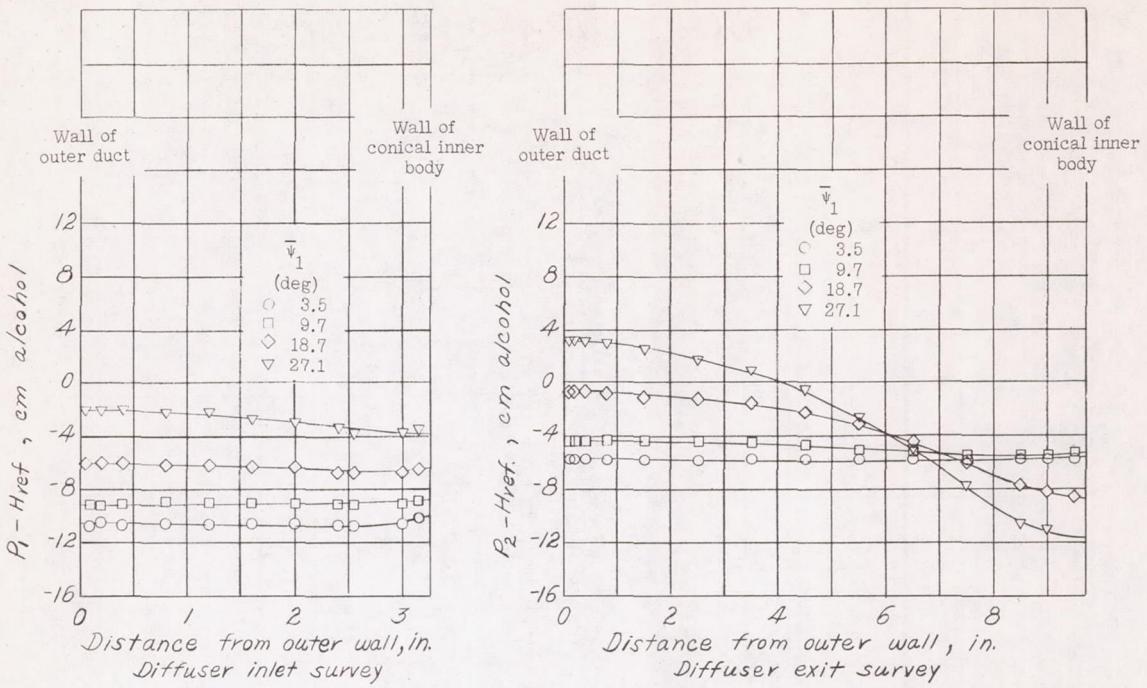

(a) Static-pressure distributions for a diffuser inlet Mach no. of 0.10.

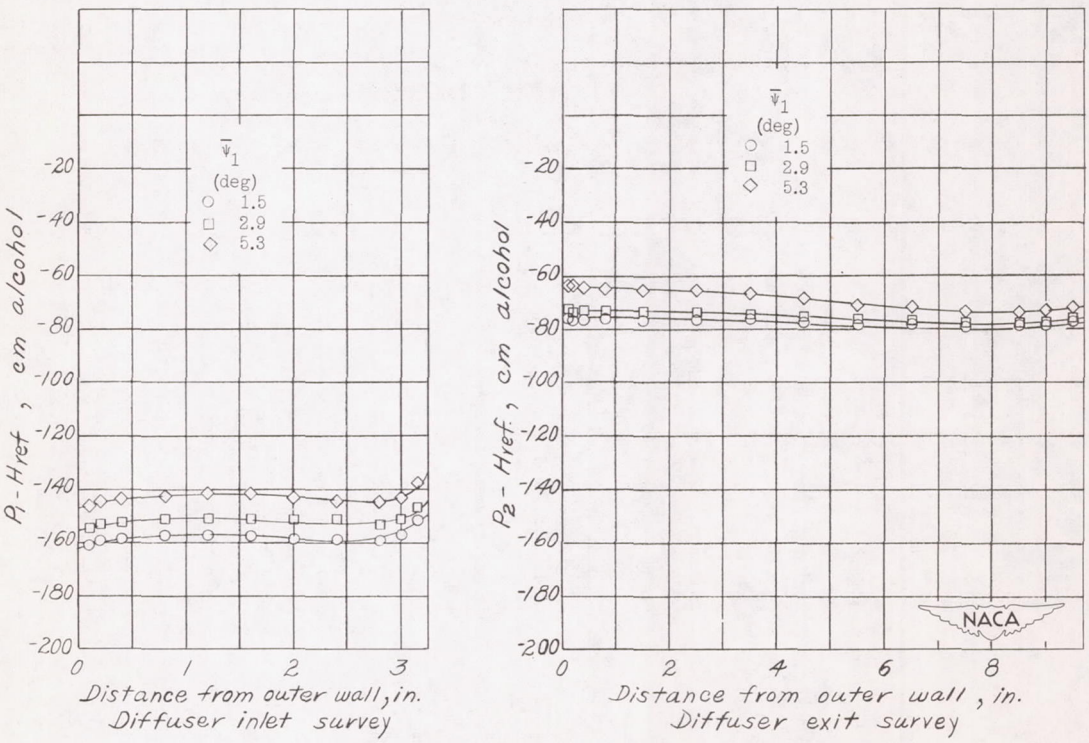

(b) Static-pressure distributions for a diffuser inlet Mach no. of 0.40.

Figure 13.- Plots of static-pressure-distribution surveys at the inlet and exit of the 16° diffuser.

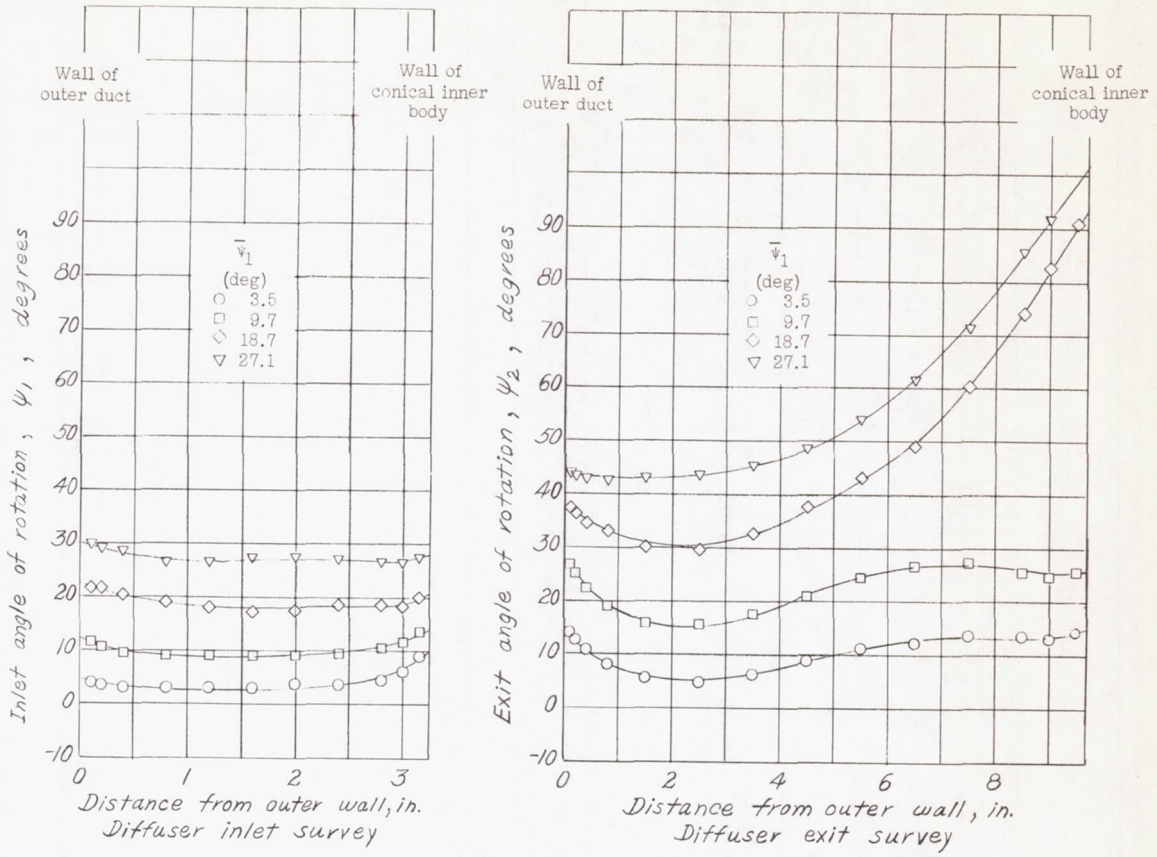

(a) Angle-of-rotation distributions for a diffuser inlet Mach no. of 0.10.

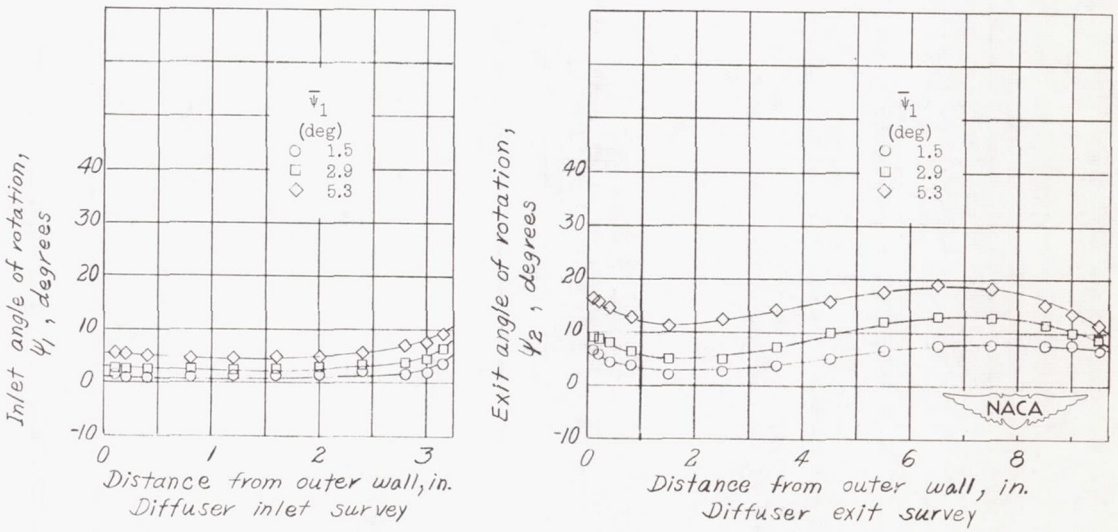

(b) Angle-of-rotation distributions for a diffuser inlet Mach no. of 0.40.

Figure 14.– Plots of angles of flow rotation at the inlet and exit of the 16° diffuser.

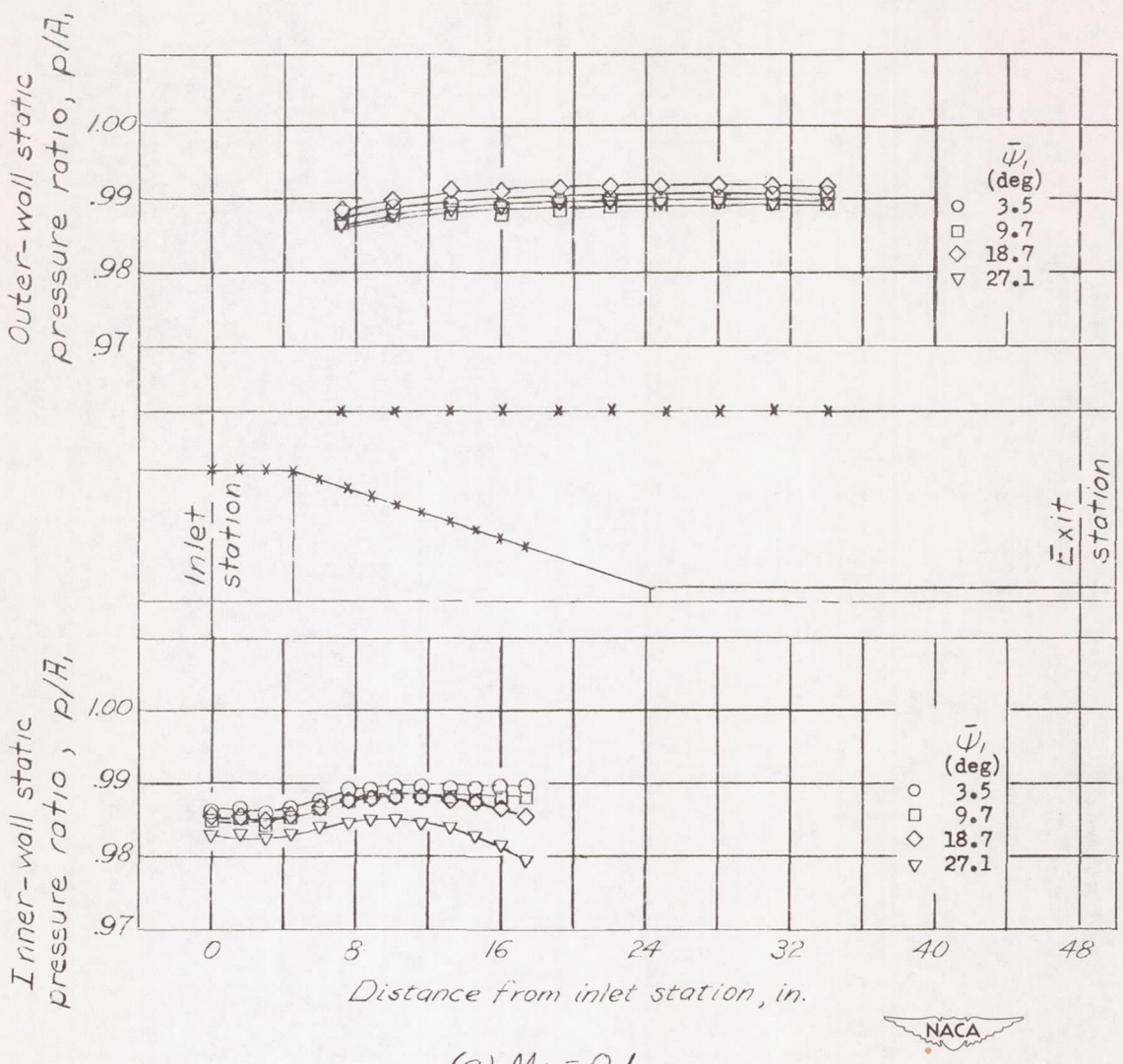

(a) $M_1 = 0.1$.

Figure 15.– Plots of wall static pressures along inner conical body and outer duct for the 16° diffuser.

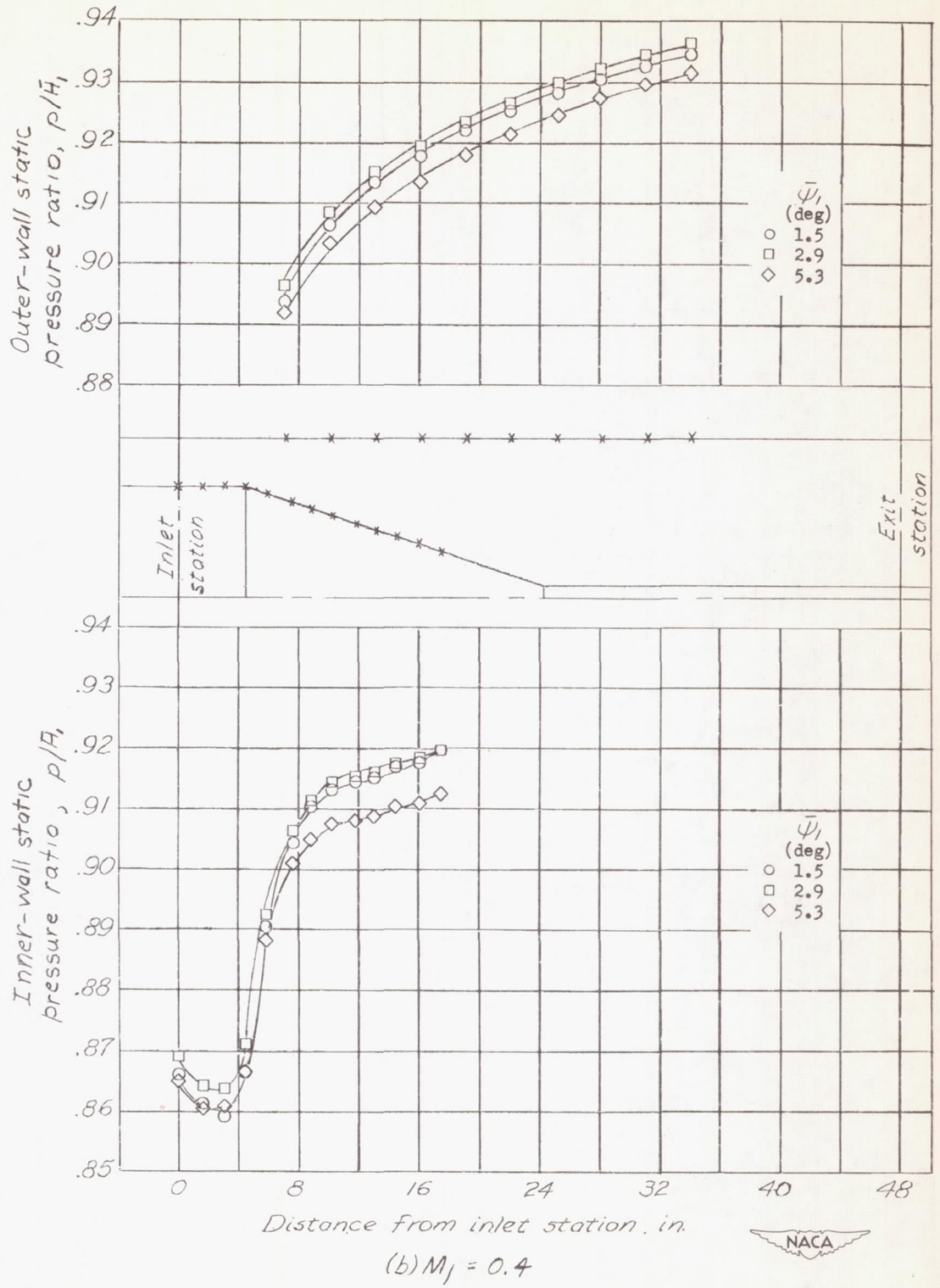

(b) $M_1 = 0.4$

Figure 15.– Concluded.